Acta Biomaterialia 10 (2014) 1443–1450

Contents lists available at ScienceDirect

Acta Biomaterialia

journal homepage: www.elsevier.com/locate/actabiomat

Furthering the understanding of silicate-substitution in α-tricalcium phosphate: An X-ray diffraction, X-ray fluorescence and solid-state nuclear magnetic resonance study

J. Duncan [a,*], S. Hayakawa [b], A. Osaka [b], J.F. MacDonald [c], J.V. Hanna [c], J.M.S. Skakle [a], I.R. Gibson [a,d]

[a] Department of Chemistry, University of Aberdeen, UK
[b] Department of Bioscience and Biotechnology, University of Okayama, Japan
[c] Department of Physics, University of Warwick, UK
[d] Institute of Medical Sciences, University of Aberdeen, UK

ARTICLE INFO

Article history:
Received 13 August 2013
Received in revised form 24 October 2013
Accepted 17 November 2013
Available online 25 November 2013

Keywords:
$Ca_3(PO_4)_2$
Silicon
Bioceramics
Rietveld
^{29}Si
^{31}P

ABSTRACT

High-purity (SupT) and reagent-grade (ST), stoichiometric and silicate-containing α-tricalcium phosphate (α-TCP: ST0/SupT0 and Si-TCP $x = 0.10$: ST10/SupT10) were prepared by solid-state reaction based on the substitution mechanism $Ca_3(PO_4)_{(2-x)}(SiO_4)_x$. Samples were determined to be phase pure by X-ray diffraction (XRD), and Rietveld analysis performed on the XRD data confirmed inclusion of Si in the α-TCP structure as determined by increases in unit cell parameters; particularly marked increases in the *b*-axis and β-angle were observed. X-ray fluorescence (XRF) confirmed the presence of expected levels of Si in Si-TCP compositions as well as significant levels of impurities (Mg, Al and Fe) present in all ST samples; SupT samples showed both expected levels of Si and a high degree of purity. Phosphorus (^{31}P) magic-angle-spinning solid-state nuclear magnetic resonance (MAS NMR) measurements revealed that the high-purity reagents used in the synthesis of SupT0 can resolve the 12 expected peaks in the ^{31}P spectrum of α-TCP compared to the low-purity ST0 that showed significant spectral line broadening; line broadening was also observed with the inclusion of Si which is indicative of induced structural disorder. Silicon (^{29}Si) MAS NMR was also performed on both Si-TCP samples which revealed Q^0 species of Si with additional Si Q^1/Q^2 species that may indicate a potential charge-balancing mechanism involving the inclusion of disilicate groups; additional Q^4 Si species were also observed, but only for ST10. Heating and cooling rates were briefly investigated by ^{31}P MAS NMR which showed no significant line broadening other than that associated with the emergence of β-TCP which was only realised with the reagent-grade sample ST0. This study provides an insight into the structural effects of Si-substitution in α-TCP and could provide a basis for understanding how substitution affects the physicochemical properties of the material.

1. Introduction

Various calcium phosphate materials have generated significant interest as potential biomaterials due to their chemical and structural similarities to the calcium phosphate apatite phase that is the mineral component of natural bone. Materials such as tricalcium phosphate (TCP: $Ca_3(PO_4)_2$) have been subject to increased attention recently since this compound demonstrates both resorbable and bioactive characteristics, meaning that it will interact readily with the hard tissues of the human body and may eventually be completely replaced by natural bone [1,2]. TCP can exist in a number of crystallographic forms, with the alpha (α-TCP) and beta (β-TCP) polymorphs, which correspond to high- and low-temperature phases respectively, being the most extensively studied [3,4]. When compared with β-TCP, α-TCP has a much more open structure [4], is thus less dense and has a higher free energy of formation [5], it exhibits greater solubility [6], and can also act as a bone cement through its propensity to react with water to form a calcium-deficient apatite [7–9]; this intrinsic resorbability property allows it to be entirely replaced by the host's own tissues. These properties can be a distinct advantage over stoichiometric hydroxyapatite (HA) implants, which are essentially insoluble and can remain unaltered after implantation [10–12].

The challenge with using α-TCP as a ceramic is that it is a metastable phase at room temperature; this means that the α-TCP structure needs to be frozen in place from the high temperatures where it exists as a thermodynamically stable phase. If a sample of TCP is heated to ~1150 °C (or above, up to ~1450 °C) [3] and allowed to cool slowly, the crystal structure can alter from α-TCP to

* Corresponding author. Tel.: +44 1224 272196.
E-mail address: jo.duncan@abdn.ac.uk (J. Duncan).

1742-7061/$ - see front matter © 2013 Acta Materialia Inc. Published by Elsevier Ltd. All rights reserved.
http://dx.doi.org/10.1016/j.actbio.2013.11.014

form β-TCP. In practice, this implies that sample preparations need to be removed from high-temperature furnaces and quenched rapidly to room temperature to ensure that the α-TCP polymorph is retained.

The addition of various dopants into the TCP lattice has been shown to alter the β–α transition temperature. Magnesium is known to stabilise the β-form to higher temperatures [13,14] which enables β-TCP to be heated to temperatures higher than its usual upper limit of stability (~1150 °C) to promote densification without conversion to the less dense α-polymorph. In contrast, the addition of Si helps to stabilise α-TCP to a lower temperature [15–19], effectively rendering α-TCP easier to make in the laboratory as sample quenching then becomes less important. Recent studies have highlighted the effect of magnesium impurities on the phase composition of mixtures of Si-stabilised α-TCP (Si-TCP) and HA, with 250–300 ppm magnesium significantly increasing the amount of β-TCP that forms at the expense of the Si-TCP phase [20].

In addition to the stabilising effect on the α-TCP structure, Si is also an essential trace element for bone growth [21–23] and Si has also been shown to significantly enhance the bioactivity of HA implants when substituted for phosphate ions in the HA structure [24,25]. Silicate ions have been shown to substitute into the HA lattice to form substituted single-phase ceramics with compositions containing between 0 and 1.6 wt.% Si [26]. The compositional range that describes silicate ion substitution into the α-TCP structure, without the formation of secondary phases detectable by X-ray diffraction (XRD) analysis, was reported as between 0.59 and 1.14 wt.% Si, using an aqueous precipitation reaction [15] which followed on from a previous study [16]. Samples were produced by precipitating an apatite with a calcium to phosphorus (Ca/P) molar ratio of between 1.50 and 1.70 in ammoniated solutions and adding between 0 and 2.26 wt.% fused silica to the precipitate to maintain a calcium to phosphorus + silicon (Ca/(P + Si)) molar ratio of 1.50; dried samples were sintered for 2 h at 1250 °C. The authors found that Si compositions below 0.59 wt.% produced multiphase compositions (Si-TCP, β-TCP and HA), and for compositions with more than 1.14 wt.% Si biphasic compositions of Si-TCP and HA were obtained. More recently, a single-phase Si-TCP phase has been produced by other groups, using solid-state synthesis [18] and aqueous precipitation methods [2,18] (at 1.3 and 0.9 wt.% silicate substitution for the respective references). The substitution of silicon for phosphorus into a tricalcium phosphate cement was also found to increase the cement's rate of hydrolysis which was attributed to increased solubility [27].

In the current study, an investigation of the chemical structure of both α-TCP and Si-TCP samples with very high levels of chemical purity was performed with the aim of identifying the effect of synthesis conditions on the structure of these final compositions. Previous ^{31}P magic-angle-spinning nuclear magnetic resonance (MAS NMR) characterisation of α-TCP formed under solid-state synthesis conditions using HA and anhydrous dicalcium phosphate as precursors [5] reported products that are inconsistent with well-established structures [3]; this study proposed that a network comprising 15 chemically independent phosphorus positions resulted from such a synthetic route. The present study aims to demonstrate by ^{31}P MAS NMR investigation that α-TCP formed through a solid-state synthesis route using high-purity $CaCO_3$ and $CaHPO_4$ as precursors generates well-formed phases that are completely consistent with the monoclinic 12 phosphorus site model proposed by Mathew et al. [3]. This initial structural characterisation will act as a baseline for understanding the α-TCP network, especially when direct incorporation of various ions into the lattice is attempted. In the current study, the effect of the substitution of Si onto a P site in the α-TCP structure will be investigated by both ^{31}P and ^{29}Si MAS NMR, making use of a ^{29}Si isotope-enriched precursor in an attempt to understand the structural differences of Si-substituted compositions compared with stoichiometric α-TCP.

2. Methods and materials

2.1. Synthesis of TCP compositions

Samples of stoichiometric α-TCP ($x = 0.00$) and Si-TCP ($x = 0.10$) were prepared based on the following chemical equation:

$$(1+x)CaCO_3 + (2-x)CaHPO_4 + xSiO_2 \rightarrow \text{“Si}-\text{TCP”}: (Ca_3P_{2-x}Si_xO_{8-x/2}) + (CO_2 + H_2O) \quad (1)$$

High-purity stoichiometric α-TCP (SupT0) was synthesised by solid-state reaction using methods similar to those previously reported [4,9,18,28] by grinding together (in acetone) analytical-grade $CaCO_3$ (Sigma Aldrich, UK) and high-purity $CaHPO_4$ in a 1:2 M ratio that was then subject to a heating step described below. The $CaHPO_4$ was produced by methods described elsewhere [29]; briefly, an H_3PO_4 solution (VWR, UK), was added rapidly into a suspension of $Ca(OH)_2$ (VWR, UK) at 70 °C and pH ~5 to form a precipitate with a Ca/P molar ratio of 1.00 that was subsequently filtered and dried at ~80 °C overnight. General-purpose reagent-grade $CaCO_3$ and $CaHPO_4$ (both Sigma Aldrich, UK) were used to synthesise the sample ST0 by employing the same methods.

For a high-purity Si-containing sample ($x = 0.10$, SupT10), ^{29}Si isotopically enriched (99.33%) SiO_2 (provided by the University of Warwick) was added at the expense of high-purity $CaHPO_4$ with the less-pure sample ($x = 0.10$, ST10) being synthesised using fumed SiO_2 (BDH Laboratories, UK), at the expense of commercially available $CaHPO_4$ (Sigma Aldrich, UK). The loss of calcium was then compensated for by addition of more $CaCO_3$ (Sigma Aldrich, UK) so that the Ca/(P + Si) molar ratio of samples remained at 1.50.

Grinding of reactants was followed by a 16 h heating step in a muffle furnace (Carbolite, UK) at 1300 °C in air. Post-heat treatment, samples were subject to a further regrinding and reheating at 1300 °C for 8 h in order to ensure homogeneity of reactants and promote complete reaction. Samples were quenched from 1300 °C to room temperature in air, using a brass quenching block.

2.2. X-ray diffraction and Rietveld analysis

The phase purity of samples was determined (with reference to α-TCP, ICDD card No. 09-348) by XRD using a D8 Advance diffractometer (Bruker, DE) with Cu $K_{\alpha 1/2}$ radiation; for Rietveld analysis, data were collected on samples ST0, SupT0 and ST10 over 5°–100° 2θ with a step size of 0.02° (total collection time >12 h). SupT10 was analysed on an XPert Pro MPD (PANalytical, NL) equipped with a solid-state PIXcel detector using Cu $K_{\alpha 1}$ radiation and a 0.013° step size (total collection time >15 h).

Rietveld analysis was performed on XRD patterns of samples using the software package TOPAS Academic. The crystallographic starting model used in refinement was based on a calculated diffraction pattern (ICDD 29-359) produced by data from Mathew et al. [3] based on a monoclinic unit cell. This is similar to the experimental data (ICDD card No. 09-348) [30] which tended to be used for quick phase identification.

Due to the highly complex nature of the α-TCP structure, a full refinement was not attempted and only values such as machine parameters, background/peak-shape functions, unit cell dimensions and atomic positions were refined. Silicon was not incorporated into the model for Si-containing samples due to the inability of X-rays to differentiate between silicon and phosphorus. Thermal parameters can absorb the effects of atomic position and so these were not refined either.

2.3. X-ray fluorescence spectroscopy

To determine, quantitatively, levels of Si and the purity of the samples, X-ray fluorescence (XRF) was performed on a selection of samples; samples were analysed by Ceram (Stoke-on-Trent, UK) using the fused bead method to prepare samples for analysis.

2.4. Magic-angle-spinning nuclear magnetic resonance spectroscopy

^{29}Si and ^{31}P MAS NMR measurements were performed at ambient temperatures (~297 K) on a Varian Infinity Plus 300 spectrometer (B_0 = 7.05 T) operating at Larmor frequencies of 59.6 and 121.5 MHz for ^{29}Si and ^{31}P, respectively.

Single-pulse ^{29}Si MAS experiments were implemented using a Bruker 7 mm double-air-bearing probe in which MAS frequencies of 5 kHz were achieved using ZrO_2 rotors. A $\pi/4$ pulse time of 3 μs and long recycle delays of 480 s were common to all measurements to ensure a quantitative description of the Si speciation (total collection time of ~17 h). The reported ^{29}Si chemical shifts are referenced against the primary reference of trimethlysilane (δ 0.0 ppm) using a secondary solid standard of kaolinite at δ −92 ppm. Single-pulse ^{31}P experiments were undertaken using a Bruker double-air-bearing 4 mm MAS probe in which MAS frequencies of 12 kHz were achieved using ZrO_2 rotors. A $\pi/4$ pulse length of 2 μs and a recycle delay of 300 s was used (total collection time of ~20 min), with all ^{31}P chemical shifts referenced against 85% H_3PO_4 (δ 0.0 ppm) via solid $NH_4H_2PO_4$ at δ 0.9 ppm.

The DMfit software package was used for all deconvolutions and simulations of the experimental NMR data [31].

3. Results and discussion

3.1. Phase compositions: XRD and Rietveld analysis

All samples produced in this study were single phase with only an α-TCP phase being observed in all diffraction patterns (to the limits of detection by XRD). An example of a diffraction pattern, refined pattern and residual following Rietveld refinement for samples SupT0 and SupT10 are shown in Fig. 1 in the upper and lower images, respectively; note, the range reported is shown from 10° to 60° 2θ for ease of viewing.

Values for unit cell parameters and cell volume from Rietveld analysis of diffraction data from SupT and ST samples are listed in Table 1; the unit cell dimensions for sample SupT0 were the nearest to the expected values elucidated by Yashima et al. [32] (their refined values came from synchrotron powder diffraction data and utilised the same starting model as proposed by Mathew et al. [3].)

The substitution of Si into the α-TCP structure results in an increase in all unit cell parameters, with the greatest increases observed for the b-axis length and the β-angle. These increases are comparable to what was observed by Reid et al. [15]. These data suggest that Si is, at least in part, incorporated into the crystal lattice of the α-TCP structure and that, due to larger increases in dimensions, high-purity (SupT) samples are either more receptive to Si-substitution than less pure (ST) samples, or that the effects of doping are more readily observed when chemical impurities are minimised. Failing to include Si in the model for refinements should not affect the unit cell values obtained because unit cell dimensions are related to peak positions (i.e. the d-spacing of a given plane), whereas scattering atom type is related to peak intensity; because silicon and phosphorus are very difficult to distinguish from one another by powder XRD, the differences in peak intensity are not readily appreciated.

3.2. Chemical composition analysis: XRF

The chemical composition of samples as elucidated by XRF is shown in Table 2.

The Si weight percentage calculated from XRF data acquired on SupT and ST samples revealed that the Si contents of samples were near the expected values, suggesting that the composition of the product is easily tailored using solid-state methods; SupT samples showed ideal levels of Si inclusion (0.00 and 0.91 wt.% for x = 0.00 and 0.10, respectively); ST samples showed a Si impurity at x = 0.00 and a slightly lower than expected value for x = 0.10 (0.09 and 0.84 wt.% respectively).

Impurity levels were calculated from XRF data and showed that SupT samples contained no impurities above the levels of detection (0.02 wt.% as oxides) and the contribution from trace element impurities in ST samples comprised levels of magnesium of 0.22 and 0.09 wt.% for ST0 and ST10, respectively, with lesser contributions from aluminium (0.05 and 0.02 wt.%) and iron (0.03 and 0.02 wt.%); it is unclear what form these impurities exist as (as oxides these would be below the levels detectable by XRD).

It is highly likely that the commercial monetite used in the synthesis is the main source of the magnesium impurity; supporting evidence for this can be found in a previous study of the effect of monetite source on the chemical and phase composition of α-TCP [29]. As magnesium is known to stabilise β-TCP, it is imperative to minimise the magnesium content in reactants to ensure full transformation to α-TCP. This is supported by a study showing the effect of magnesium impurities on forming biphasic Si-TCP/HA compositions [20].

3.3. MAS NMR spectroscopy characterisation

The data shown as the uppermost trace in Fig. 2 demonstrate that a very high-resolution ^{31}P MAS NMR spectrum is achievable when using high-purity $CaCO_3$ and $CaHPO_4$ precursor powders to synthesise stoichiometric α-TCP (SupT0) via conventional solid-state routes. The deconvolution of this data, shown in Fig. 2 as the middle trace (model) and lowermost traces (individual deconvoluted peaks) and summarised in Table 3, reveals that 12 sharp, distinct ^{31}P chemical shifts in the Q^0-range can be resolved and measured; this result corroborates the X-ray structural solution for α-TCP reported by Mathew et al. [3] that proposed 12 chemically independent P positions in the monoclinic unit cell of α-TCP. The 12 sites should all have the same integrated intensity value and the discrepancy of values is likely due to the deconvolution procedure rather than an actual physical reason.

The ^{31}P MAS NMR spectrum acquired for SupT10 (Fig. 3, uppermost trace) suggested that the incorporation of Si onto a P position induces a large degree of line broadening; a model was constructed which consisted of four Gaussian components in the Q^0-range after the deconvolution procedure (Fig. 3 and Table 3). The ^{29}Si MAS NMR data for sample SupT10 (Fig. 4) shows a narrow distribution of Q^0 speciation with lower concentrations of Q^1/Q^2 species (Si Q^0 species have been reported to have chemical shifts ranging from −69 to −75 ppm [33,34], Q^1 species from approximately −77 to −83 ppm and Q^2 from −86 to −87 ppm [35]).

The optimal deconvolution of this spectrum, displayed in Fig. 5 and detailed in Table 4, was best achieved using line-shapes with a 50:50 mixed Lorentzian and Gaussian character. The spectrum was deconvoluted to four components in the Q^0 range and four components in the Q^1/ Q^2 range at −75.89, −77.67, −84.46 and −86.3 ppm. The latter two of these values are similar to the Q^2 Si species encountered in pseudowollastonite (α-$Ca_3Si_3O_9$) quoted as −84.2 ppm [36] or in wollastonite at −88 ppm [33], whereas the former two are similar to what was assigned as a Q^0 environment in Si-TCP (−76.7 ppm) in a biphasic HA–TCP system substituted

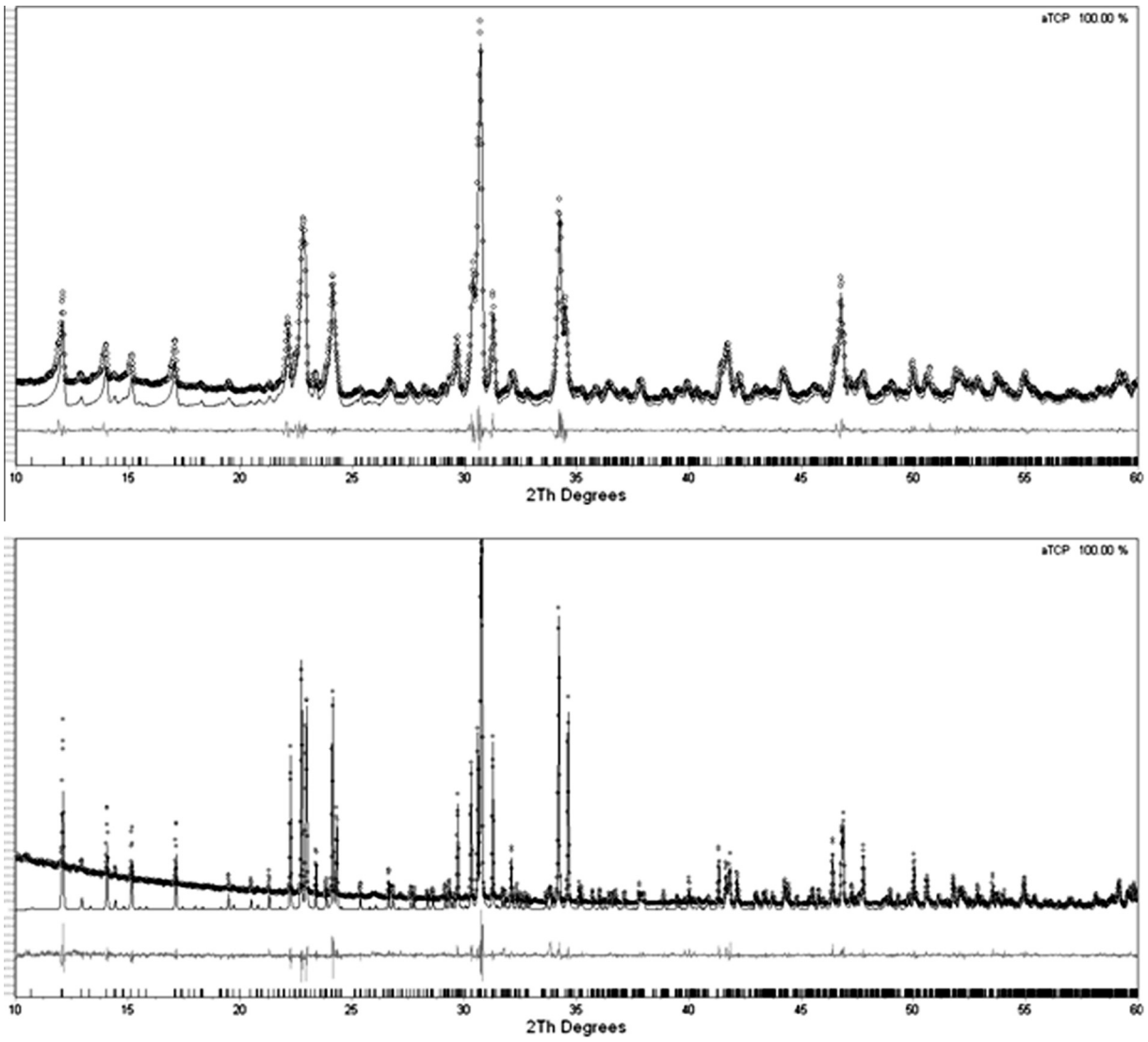

Fig. 1. TOPAS Academic output showing the X-ray diffraction pattern (dots), refined pattern following Rietveld analysis (black line) and the difference curve (grey line) of high-purity α-TCP sample SupT0 (upper image) and SupT10 (lower image).

Table 1
Unit cell parameters obtained from Rietveld refinement of X-ray diffraction data of stoichiometric and Si-substituted α-TCP samples. Data are shown to a number of decimal places relevant the error; errors are rounded estimated standard deviations from TOPAS. Data are for high-purity ($x = 0.00$; SupT0 and $x = 0.10$; SupT10) and reagent-grade ($x = 0.00$; ST0 and $x = 0.10$; ST10) samples.

	a (Å)	b (Å)	b (Å)	β (°)	V (Å^3)
SupT0	12.8754(9)	27.2676(19)	15.2131(10)	126.168(2)	4311.7(5)
SupT10	12.8839(2)	27.3862(3)	15.2381(2)	126.376(8)	4328.7(1)
ST0	12.864(3)	27.321(5)	15.219(3)	126.282(6)	4311.6(15)
ST10	12.8685(14)	27.340(3)	15.2218(16)	126.397(3)	4310.7(8)

Table 2
Impurity levels calculated from XRF data collected on α-TCP (low-purity, ST0; high-purity, SupT0) and Si-substituted α-TCP samples (low-purity, ST10; high-purity, SupT10).

	Si (wt.%)	Mg (wt.%)	Al (wt.%)	Fe (wt.%)
SupT0	0.00	0.00	0.00	0.00
SupT10	0.91	0.00	0.00	0.00
ST0	0.09	0.22	0.05	0.03
ST10	0.84	0.09	0.02	0.02

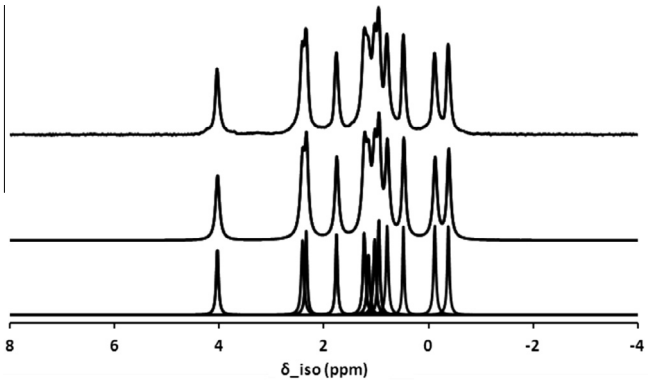

Fig. 2. Deconvolution of ^{31}P spectra for high-purity α-TCP ($x = 0.00$, SupT0); raw spectrum is the uppermost trace, the constructed model is shown in the centre and the individual Lorentzian peaks constituting the model are shown as the lowermost traces.

Table 3
Numerical data following deconvolution of 31P MAS NMR spectra of high-purity samples of α-TCP (x = 0.00; SupT0) using Lorentzian peak shapes and Si-TCP (x = 0.10; SupT10) using Gaussian peak shapes.

Sample	Position (ppm)	FWHM (ppm)	Integrated intensity (A.U.)	Sample	Position (ppm)	FWHM (ppm)	Integrated intensity (A.U.)
SupT0	-0.38	0.08	723	SupT10	0.72	2.40	32125
	-0.12	0.09	741		2.39	1.23	7162
	0.48	0.07	739		3.37	1.41	5725
	0.79	0.09	816		4.20	2.77	2770
	0.95	0.08	775				
	1.03	0.10	779				
	1.15	0.10	618				
	1.23	0.10	846				
	1.76	0.08	699				
	2.33	0.08	676				
	2.41	0.10	767				
	4.04	0.09	595				

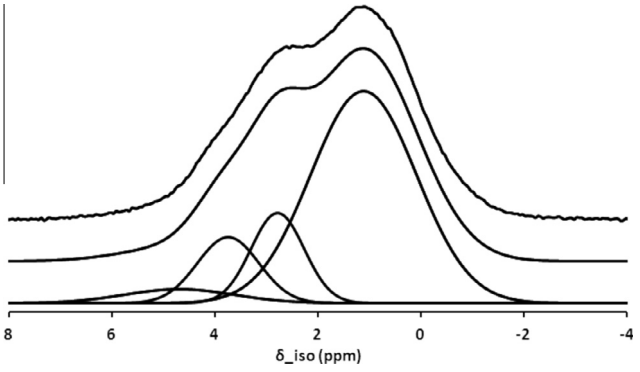

Fig. 3. Deconvolution of ^{31}P spectra for high-purity Si-TCP (x = 0.10, SupT10); raw spectrum is the uppermost trace, the constructed model is shown in the centre and the individual Gaussian peaks constituting the model are shown as the lowermost traces.

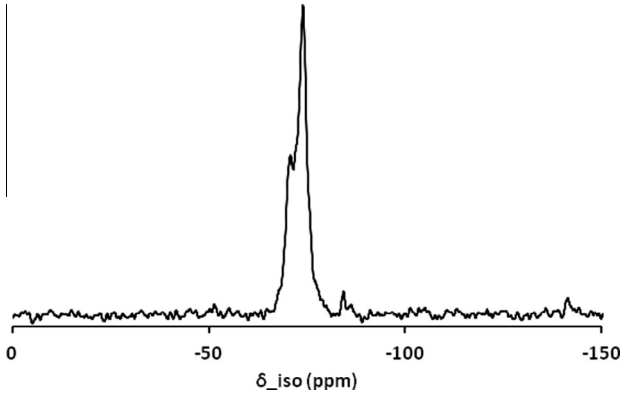

Fig. 4. ^{29}Si MAS NMR spectrum of high-purity ^{29}Si-enriched sample of Si-TCP (x = 0.10; SupT10).

with Si [36] which yielded a ^{29}Si spectrum that was qualitatively quite similar to what was found in the current study.

The ^{31}P MAS NMR spectra for samples ST0 and ST10 consisted of entirely Q^0 orthophosphate species (~0–4 ppm) and are shown as the uppermost traces in Figs. 6 and 7. For ST0, the ^{31}P spectrum shows three broad resonances with additional shoulder features observed at ~0 ppm.

These broad resonances suggest a certain amount of structural disorder and/or paramagnetic broadening due to the presence of Fe_2O_3 in the sample. ST10 shows a further loss of resolution in the phosphorus environments when Si is substituted into the

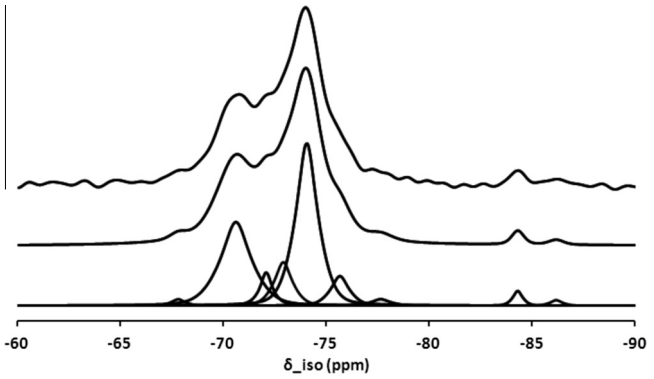

Fig. 5. Deconvolution of ^{29}Si spectrum for high-purity, ^{29}Si-enriched Si-TCP (x = 0.10, SupT10). Raw spectrum is the uppermost trace, the constructed model is the shown in the centre and the individual peaks (of a 50:50 mixed Gaussian:Lorentzian character) are shown as the lowermost traces.

Table 4
Numerical data following deconvolution of ^{29}Si MAS NMR spectrum for high-purity Si-TCP (x = 0.10, SupT10) using 50:50 mixes of Gaussian and Lorentzian peaks.

Sample	Position (ppm)	FWHM (ppm)	Integrated intensity (A.U.)
SupT10	−68.20	1.04	154
	−70.70	2.30	5903
	−72.47	2.10	3952
	−74.20	2.12	11738
	−75.89	1.66	1479
	−77.67	3.74	1647
	−84.46	1.15	461
	−86.30	1.68	350

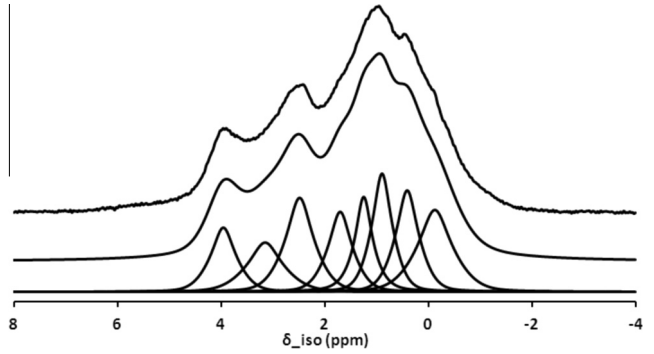

Fig. 6. Deconvolution of ^{31}P spectra for α-TCP (ST0) using 50:50 mixes of Gaussian and Lorentzian functions. Raw spectrum is the uppermost trace, the constructed model is shown in the centre and the individual peaks constituting the model are shown as the lowermost traces.

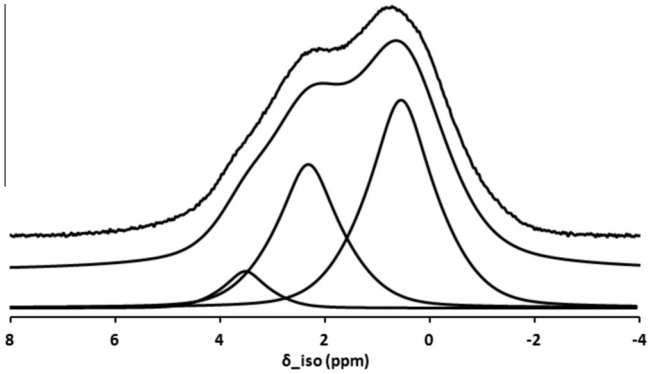

Fig. 7. Deconvolution of ^{31}P spectra for Si-TCP (x = 0.10; ST10) using 50:50 mixes of Gaussian and Lorentzian functions. Raw spectrum is the uppermost trace, the constructed model is shown in the centre and the individual peaks constituting the model are shown as the lowermost traces.

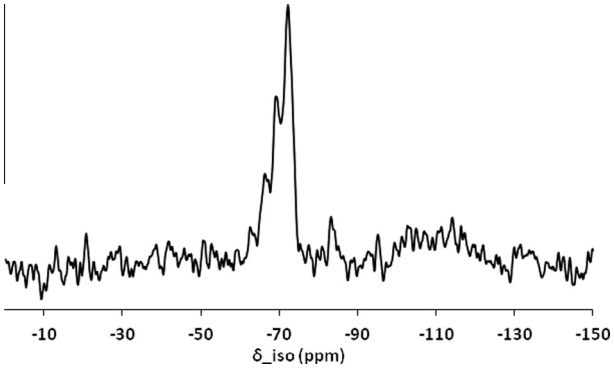

Fig. 8. ^{29}Si MAS NMR spectrum of reagent-grade sample of Si-TCP (x = 0.10; ST10).

structure as only two broad features are readily delineable (upper line).

Spectral deconvolution of the ^{31}P spectra of ST0 and ST10 was achieved by employing a model consisting of a 50:50 mix of Gaussian and Lorentzian peak shape functions. A suite of eight resonances was found to reconstruct the observed manifold of signals for ST0 and, similarly, three resonances could reconstruct the highly broadened spectrum of ST10; see Fig. 7 and Table 5.

The ^{29}Si MAS NMR data for sample ST10 (Fig. 8) indicates the presence of multiple Q^n species, with Q^0, Q^1/Q^2 and Q^3/Q^4 species detected. Following a deconvolution process limited to the near Q^0 region utilising line-shapes of pure Gaussian character, four resonances were found at approximately −63.2, −66, −69.3 and −72.3 ppm with an additional resonance at approximately -75.6 ppm which falls slightly outside of the literature reported Q^0 range. Additionally, a resonance at −83.3 ppm was found which could correspond to Q^1/Q^2. A broad resonance in the Q^3–Q^4 region (around −100 to −120 ppm) is indicative of Si present in a glassy/amorphous SiO_2 phase. The distribution of phosphorus resonances of ST10 in Fig. 7 (Q^0 only), suggests that the amorphous phase that has formed is entirely silicate based. Inferring a relative amount to which the Si exists in this form could potentially be erroneous as the significantly longer T1-times that can emanate from SiO_2-type structures might lead to an underrepresentation of these resonances due to saturation of these ^{29}Si species from the recycle delays employed in this study.

The ^{29}Si data for SupT10 (Fig. 4) shows a simpler distribution of speciation; the low field resonances at around −100 to −120 ppm are nearly absent and a much narrower distribution of Q^0 speciation exists when impurities have been eliminated; the proposed Q^1/Q^2 species are still present and are resolvable to two environments. Isotopic labelling (^{29}Si) was employed in the synthesis of the SupT10 sample and the superior spectral SNR obtained afforded easier observation of lower-intensity species and more accurate simulation and deconvolution of the ^{29}Si line-shape when compared to ST10.

The ^{29}Si MAS NMR spectra suggest that the Si that is directly incorporated into the lattice is somewhat evenly distributed across the various phosphate sites based on the multiple Q^0 environments. However, studies undertaken by Rawal et al. [37] found that for β-TCP (co-substituted with Zn and Si) the majority of the Si (60%) was not incorporated into the lattice, but existed as nano-inclusions consisting of a range of Q^0, Q^1 and Q^2 species. In their study Zn and Si were substituted at 5 and 10 mol.%, which relates to values of x in Eq. (1) of 0.1 and 0.2, respectively, but with Zn substituting for Ca at 0.15 and 0.3, respectively. The phase composition of both of these was entirely β-TCP for the 10 mol.% substituted sample with a minor amount of α-TCP in the 5 mol.% substituted sample. The ^{29}Si MAS NMR data obtained for ST10 at natural abundance in Fig. 8 can be compared to the ^{29}Si MAS NMR data for Si-TCP reported by Langstaff et al. [17] which yielded no ^{29}Si signal even after using 95% isotopically labelled $^{29}SiO_2$ as the enrichment precursor; however, the synthesis scheme was based on an aqueous method with thermal processing of the precipitate.

A more recent study by Gillespie et al. [38] prepared Si-TCP by an aqueous precipitation reaction based on previous methods [6,15,20], combining ammonium phosphate and calcium nitrate under alkali conditions, introducing Si to the reaction by adding a ^{29}Si-enriched silica powder, which was different to the finely dispersed fumed silica colloid used in this group's previous studies [15,20,39]. The composition of their product material was not single phase, with a composition of 90% Si-TCP and 10% HA being reported, but their final product did contain a level of Si comparable to that reported for composition ST10 in the present study. The ^{29}Si MAS NMR study of their composition showed two resonances at chemical shifts of −75.2 and −78.0 ppm, and the authors proposed that the latter was due to a Q^1 silicate structure and the former to either Q^0 or Q^1. In their study they predicted ^{29}Si chemical shifts for

Table 5
Numerical data following deconvolution of ^{31}P MAS NMR spectra for reagent-grade samples of α-TCP (ST0) and Si-TCP (x = 0.10, ST10) using 50:50 mixes of Gaussian and Lorentzian peaks.

Sample	Position (ppm)	FWHM (ppm)	Integrated intensity (A.U.)	Sample	Position (ppm)	FWHM (ppm)	Integrated intensity (A.U.)
ST0	−0.12	1.01	5218	ST10	0.55	1.96	27824
	0.41	0.68	4415		2.32	1.86	18360
	0.90	0.60	4541		3.52	1.29	3352
	1.25	0.61	3707				
	1.70	0.71	3628				
	2.48	0.82	4930				
	3.15	1.03	3192				
	3.95	0.75	3048				

a calcium excess and an oxygen-deficient model of Si-TCP, producing Q^0 values of -69.9 and -73.3 and Q^1 values of −71.1 and −81.1 ppm. These predicted values are closer to the observed values for ST10 of −66, −69.3 and −72.3 (proposed as being Q^0), −75.6 (proposed as Q^0/Q^1) and −83.3 ppm (proposed as Q^1/Q^2) than the observed values in their study (−75.2 and −78 ppm). A recent study by Gomes et al. [40] found that a biphasic mixture of Si-doped HA and β-TCP yielded a ^{29}Si MAS NMR spectrum with Q^0 groups assigned in the −69 to −78 ppm range, along with "condensed silicon species" expected in the −85 to −110 ppm region.

In addition to the Q^0 Si species observed in both ST10 and SupT10, there appears to be either Q^1 or Q^2 species which could potentially explain a charge-balancing mechanism, i.e. inclusion of pyrosilicate ($Si_2O_7^{6-}$).

With reference to the resolution of ^{31}P spectra, it has been observed that the addition of Si into the structure induces a loss of resolution concomitant with increased structural disorder. Comparing SupT0 with ST0 and the Si-containing samples with their stoichiometric counterparts, the disorder/broadening observed in ^{31}P spectra caused by Si incorporation at the ~1 wt.% level is more severe than that induced by either the paramagnetic broadening by Fe_2O_3 at the ~0.02–0.03 wt.% level or the structural disorder induced from general impurity levels at ~0.3 wt.% levels (or a combination of the two). Previous X-ray crystal structure studies undertaken on α-TCP describe structures characterised by 12 [3] or 16 [30] crystallographically distinct phosphorus sites, hence the number of discrete ^{31}P resonances observed in SupT0 is as one may expect, whereas for ST0 and Si-containing samples, it is much lower than expected. Thus, the full consequences of spectral broadening induced either via disorder and/or paramagnetic broadening mechanisms are demonstrated even at a very modest Si substitution and impurity levels.

The effect of heating time (4 or 8 h) was shown to correlate with the average broadening of the ^{31}P MAS NMR spectrum of α-TCP, where cooling rates of 5 or 10 °C min^{-1} were used [5]. In the current study, the heating time was considerably longer (24 h) and the cooling regime was very different (quenched in air), so the effects of heating on local structural disorder may be significant; these heating/cooling regimes were also investigated but revealed no measureable differences at 10 °C min^{-1} heating/cooling compared to air quenching other than that associated with the emergence of β-TCP (likely due to Mg-impurity; hence there were no differences in SupT samples or Si-containing samples cooled at this rate) and is shown in Fig. 9; this was only observed in the ^{31}P NMR spectrum of ST0 which developed another broad resonance at 5–6 ppm.

Despite being cooled at rates as low as 1 °C min^{-1}, the ^{31}P MAS NMR spectrum of SupT0 showed no line-broadening and is shown in Fig. 10; this suggests that line-broadening is not induced by heating/cooling regimes other than associated with that of partial conversion from α to β polymorphs.

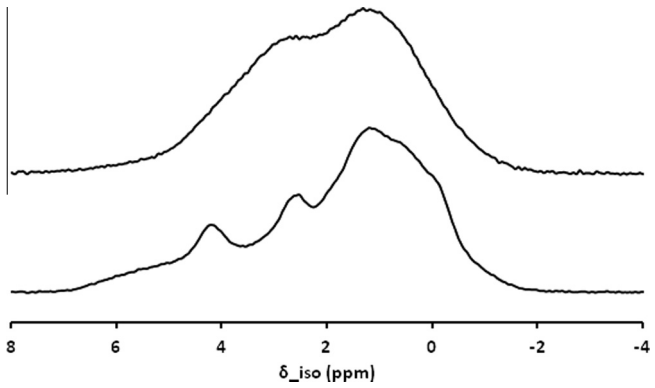

Fig. 9. ^{31}P MAS NMR spectra of reagent-grade samples of α-TCP (ST0, lower line) and Si-TCP (x = 0.10; ST10, upper line) cooled at 10 °C min^{-1}.

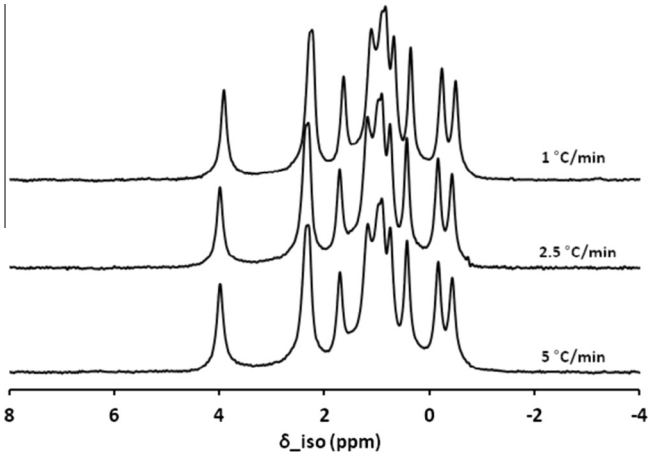

Fig. 10. ^{31}P MAS NMR spectra of high-purity samples of α-TCP (SupT0) cooled at 5, 2.5 and 1 °C min^{-1}.

4. Conclusions

Samples of Si-TCP were successfully prepared via solid-state reaction. Incorporation of Si into the crystal lattice was verified by: (i) increasing unit cell dimensions (b-axis and β-angle—determined by Rietveld analysis); (ii) expected amounts of Si detected by XRF analyses; (iii) increasing disorder observed for ^{31}P MAS NMR spectra of ST10 and SupT10 compared with their stoichiometric counterparts (ST0, SupT0); and (iv) the presence of Q^0 silicate groups (elucidated by ^{29}Si MAS NMR).

The ^{29}Si MAS NMR spectra of Si-TCP samples suggested the presence of other silicate groups such as disilicate which may reside in crystallographic sites and could potentially indicate a charge-balancing mechanism based on losing oxygen ions as shown by the following charge-balanced formula:

$$Ca_3^{2+}P_{2-x}^{5+}Si_x^{4+}O_{8-x/2}^{2-} \quad (2)$$

Acknowledgements

The authors would like to give thanks and acknowledge funding from the following bodies: a PhD studentship (J.D.) from a knowledge transfer Grant from the University of Aberdeen and Apatech Ltd. UK; the British Council (PMI-2 Scheme) which supported the research collaboration between the Universities of Aberdeen and Okayama; the Engineering and Physical Sciences Research Council (EPSRC) for the funding of an advanced research fellowship (I.G.). J.V.H. thanks EPSRC and the University of Warwick for continued support of the solid-state NMR infrastructure and acknowledges additional support for this infrastructure through Birmingham Science City: Innovative Uses for Advanced Materials in the Modern World, with contributions from Advantage West Midlands and the European Regional Development Fund.

References

[1] Hench L. J Am Ceram Soc 1998;81:1705–27.
[2] Kamitakahara M, Kurauchi T, Tanihara M, Loku K, Ohtsuki C. Key Eng Mater 2008;361-363(I):59–62.
[3] Mathew M, Schroeder LW, Dickens B, Brown WE. Acta Cryst Sec B 1977;33:1325–33.
[4] Yashima M, Sakai A. Chem Phys Lett 2003;372:779–83.

[5] Bohner M, Lemaitre J, Legrand A, De la Caillerie J-B, Belgrand P. J Mater Sci Mater Med 1996;7:457–63.
[6] Langstaff S, Sayer M, Smith T, Pugh S. Biomaterials 2001;22:135–50.
[7] Durucan C, Brown P. J Mater Sci Mater Med 2000;11:365–70.
[8] Stepuk A, Veresov A, Putlyaev V. J Phys Condens Matter 2007;19.
[9] Camiré C, Saint-Jean S, Mochales C, Nevsten P, Wang J-S, Lid- gren L, McCarthy I, Ginebra M-P. J Biomed Mater Res B 2006;76:424–31.
[10] Ogiso M, Tabata T, Ichijo T, Borgese D. J Long-Term Eff Med Imp 1992;2:235–47.
[11] Langstaff S, Sayer M, Smith TJN, Pugh SM. Biomaterials 2001;22:135–50.
[12] Mastrogiacomo M, Papadimitropoulos A, Cedola A, Peyrin F, Giannoni P, Pearce SG, Alini M, Giannini C, Guagliardi A, Cancedda R. Biomaterials 2007;28:1376–84.
[13] Kannan S, Ventura J, Ferreira J. Ceram Int 2007;33:637–41.
[14] Enderle R, Gotz-Neunhoeffer F, Göbbels M, Müller F, Greil P. Biomaterials 2005;26:3379–84.
[15] Reid J, Tuck L, Sayer M, Fargo K, Hendry J. Biomaterials 2006;27:2916–25.
[16] Reid J, Pietak A, Sayer M, Dunfield D, Smith TJN. Biomaterials 2005;26:2887–97.
[17] Langstaff S, Sayer M, Smith T, Pugh S, Hesp SAM, Thompson WT. Biomaterials 1999;20:1727–41.
[18] Massie I, Skakle J, Gibson I. Key Eng Mater 2008;361-363(I):67–70.
[19] Pietak A, Reid J, Stott M, Sayer M. Biomaterials 2007;28:4023–32.
[20] Reid J, Fargo K, Hendry J, Sayer M. Mater Lett 2007;61:3851–4.
[21] Carlisle E. J Nutr 1980;110:1046–56.
[22] Carlisle E. J Nutr 1980;110:352–9.
[23] Carlisle E. Science 1972;178:619–21.
[24] Patel N, Best S, Bonfield W, Gibson I, Hing K, Damien E, et al. J Mater Sci Mater Med 2002;13:1199–206.
[25] Patel N, Brooks R, Clarke M, Lee P, Rushton N, Gibson I, et al. J Mater Sci Mater Med 2005;16:429–40.
[26] Gibson IR, Best SM, Bonfield W. J Am Ceram Soc 2002;85:2771–7.
[27] Mestres G, Le Van C, Ginebra M-P. Acta Biomater 2012;8:1169–79.
[28] Camiré C, Gbureck U, Hirsiger W, Bohner M. Biomaterials 2005;26:2787–94.
[29] Duncan J, MacDonald JF, Hanna JV, Shirosaki Y, Hayakawa S, Osaka A, Skakle JMS, Gibson IR. Mater Sci Eng C 2013;34:123–9.
[30] Mackay AL. Acta Cryst 1953;6:743–4.
[31] Massiot D, Fayon F, Capron M, King I, Le Calvé S, Alonso B, Durand J-O, Bujoli B, Gan Z, Hoatson G. Magn Reson Chem 2002;40:70–6.
[32] Yashima M, Kawaike Y, Tanaka M. J Am Ceram Soc 2007;90:272–4.
[33] Moran G, Howe RF. Nuclear Magnetic Resonance of Geological Materials and Glasses. Encycl Anal Chem 2006.
[34] Mägi M, Lippmaa E, Samoson A, Engelhardt G, Grimmer A-R. J Phys Chem 1984;88:1518–22.
[35] Lippmaa E, Magi M, Samoson A, Engelhardt G, Grimmer AR. J Am Chem Soc 1980;102:4889–93.
[36] Gasqu'eres G, Bonhomme C, Maquet J, Babonneau F, Hayakawa S, Kanaya T, Osaka A. Magn Reson Chem 2008;46:342–6.
[37] Rawal A, Wei X, Akinc M, Schmidt-Rohr K. Chem Mater 2008;20:2583–91.
[38] Gillespie P, Wu G, Sayer M, Stott M. J Mater Sci Mater Med 2010;21:99–108.
[39] Sayer M, Stratilatov A, Reid J, Calderin L, Stott M, Yin X, et al. Biomaterials 2003;24:369–82.
[40] Gomes S, Renaudin G, Mesbah A, Jallot E, Bonhomme C, Babon- neau F, Nedelec J-M. Acta Biomater 2010;6:3264–74.